



Título artículo / Títol article: Interpretation of cyclic voltammetry measurements of thin semiconductor films for solar fuel applications.

Autores / Autors Bertoluzzi, Luca ; Badia Bou, Laura ; Fabregat Santiago, Francisco ; Giménez Juliá, Sixto ; Bisquert, Juan

Revista: The Journal of Physical Chemistry Letters

Versión / Versió: Post-print

Cita bibliográfica / Cita bibliogràfica (ISO 690): BERTOLUZZI, Luca, et al. Interpretation of Cyclic Voltammetry Measurements of Thin Semiconductor Films for Solar Fuel Applications. The Journal of Physical Chemistry Letters, 2013, vol. 4, no 8, p. 1334-1339.

url Repositori UJI: <http://hdl.handle.net/10234/89434>

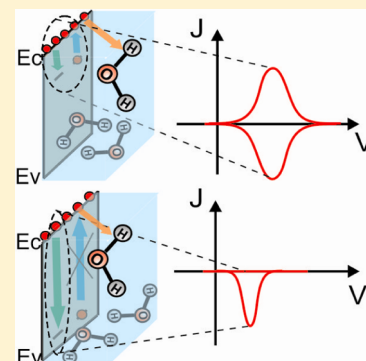
1 Interpretation of Cyclic Voltammetry Measurements of Thin 2 Semiconductor Films for Solar Fuel Applications

3 Luca Bertoluzzi, Laura Badia-Bou, Francisco Fabregat-Santiago, Sixto Gimenez, and Juan Bisquert*

4 Photovoltaics and Optoelectronic Devices Group, Departament de Física, Universitat Jaume I, 12071 Castelló, Spain

5 **S** Supporting Information

6 **ABSTRACT:** A simple model is proposed that allows interpretation of the cyclic
 7 voltammetry diagrams obtained experimentally for photoactive semiconductors with
 8 surface states or catalysts used for fuel production from sunlight. When the system is
 9 limited by charge transfer from the traps/catalyst layer and by detrapping, it is shown that
 10 only one capacitive peak is observable and is not recoverable in the return voltage scan. If
 11 the system is limited only by charge transfer and not by detrapping, two symmetric
 12 capacitive peaks can be observed in the cathodic and anodic directions. The model appears
 13 as a useful tool for the swift analysis of the electronic processes that limit fuel production.



14 **SECTION:** Energy Conversion and Storage; Energy and Charge Transport

15 **D**irect transformation of solar energy into chemical energy
 16 by hydrogen production through water splitting with
 17 semiconductor materials in a photoelectrochemical cell
 18 constitutes an attractive solution to our energy needs. However,
 19 despite the intense efforts carried out in the last decades, no
 20 single material has been identified satisfying all of the efficiency,
 21 stability, and cost conditions needed for industrial deployment
 22 of this technology.^{1–4}

23 Hematite ($\alpha\text{-Fe}_2\text{O}_3$) has emerged as a promising candi-
 24 date^{5–9} due to its abundance in the earth crust, visible light
 25 absorption, and good stability in the harsh environmental
 26 conditions needed for operation, although the obtained solar-
 27 to-fuel efficiencies still remain low for commercial exploitation.
 28 One of the main causes of the low performance of hematite is
 29 related to the large overpotentials required for water oxidation
 30 (around 500 mV), and surface treatments have proven to
 31 enhance notably water splitting performances.^{10–12} It has been
 32 suggested that the reasons for these large overpotentials are
 33 related to sluggish hole transfer to the electrolyte^{13,14} and to the
 34 existence of traps in the bulk and at the semiconductor/
 35 electrolyte interface,^{15–17} leading to high recombination.^{18,19}

36 Clearly, the separation of the different processes that constitute
 37 the oxidative current and the identification of the main kinetic
 38 bottlenecks are complex tasks. Therefore, the accurate
 39 interpretation of the results provided by characterization
 40 techniques constitutes a key tool to rationalize materials
 41 development and device optimization. Recently, we have
 42 proposed a simple physical model that allows the interpretation
 43 of impedance spectroscopy (IS) spectra for water splitting
 44 applications.²⁰ In this model, we have considered a
 45 monoenergetic level of surface states where both electron and
 46 holes can recombine or transfer from/to the solution.

47 In the present study, we propose a complementary simple
 48 model to predict the curves obtained by cyclic voltammetry
 49 (CV). This characterization technique allows a quick test of the
 50 faradaic behavior associated with charge transfer and the
 51 capacitive behavior associated with the separated modes of
 52 carrier storage, which depend on the kinetics of the system at
 53 stake.²¹ Starting from the characteristic features of reported
 54 voltammograms of hematite and related systems, we have
 55 derived a model that is able to map the different kinetic
 56 configurations of a system used for solar fuel applications. We
 57 show that two types of peaks featuring charge storage in traps
 58 can be observed when charge transfer from surface states is
 59 kinetically limited. Those peaks allow characterization of the
 60 degree of recombination at the surface states and are discussed
 61 later on.

62 In Figure 1, we present the typical voltammetry plots
 63 obtained for an Fe_2O_3 sample synthesized by atmospheric
 64 pressure chemical vapor deposition (APCVD).^{22,23} Figure 1a
 65 shows the effect of a pretreatment in dark conditions at
 66 different anodic potentials V_0 during 60 s. The voltammetry
 67 plots were recorded at a fixed scan rate (500 mV/s). This figure
 68 displays a clear cathodic capacitive peak whose height increases
 69 as the pretreatment anodic potential increases. A linear
 70 dependence exists between the peak current and V_0 , as can
 71 be seen in Figure 1b. This peak can be attributed to the
 72 charging of a monoenergetic level of surface states. It can be
 73 remarked that at a low potential (here, $V_0 = 1.66$ V versus

Received: March 13, 2013

Accepted: April 5, 2013

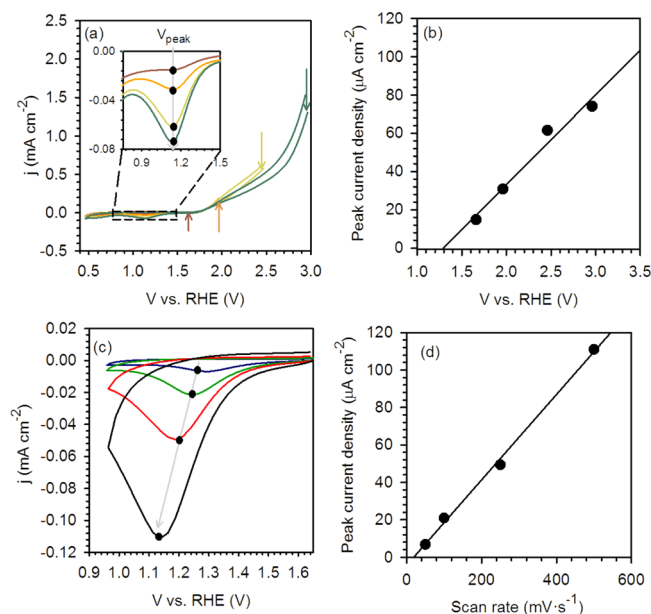


Figure 1. (a) Voltammogram of Fe_2O_3 in the dark after 60 s of pretreatment at different static potentials V_0 (indicated by arrows) at a fixed scan rate of $s = 0.5 \text{ V s}^{-1}$. Each capacitive peak occurs at the same voltage peak $V_{\text{peak}} = 1.14 \text{ V}$ versus RHE. Values of the capacitive peaks: $j_1 = 13 \mu\text{A cm}^{-2}$, $j_2 = 31 \mu\text{A cm}^{-2}$, $j_3 = 62 \mu\text{A cm}^{-2}$, and $j_4 = 74 \mu\text{A cm}^{-2}$ (b) Peak current versus voltage extracted from (a). (c) Voltammogram of Fe_2O_3 in the dark after 60 s of pretreatment under 1 sun illumination at $V_0 = 1.66 \text{ V}$ versus RHE and different scan rates (50, 100, 250, and 500 mV s^{-1}). Values of the capacitive peaks: $j'_1 = 7 \mu\text{A cm}^{-2}$, $j'_2 = 21 \mu\text{A cm}^{-2}$, $j'_3 = 49 \mu\text{A cm}^{-2}$, and $j'_4 = 111 \mu\text{A cm}^{-2}$. (d) Peak current versus the scan rate extracted from (c).

74 RHE), the cathodic peak is almost nonexistent. This indicates
75 that traps are either totally filled by electrons and emptied by
76 hole trapping when applying a high positive bias or created by
77 oxidation of the hematite surface at higher voltage. As already
78 discussed elsewhere, in the case of hematite, traps are formed
79 by forcing the oxidation of the hematite surface by applying a
80 sufficiently positive voltage.²⁴ After a pretreatment of one sun
81 illumination at the potential $V_0 = 1.66 \text{ V}$ versus RHE, the
82 cathodic peak height increases with scan rate, Figure 1c. Note
83 that the voltammetry sweep is not performed under
84 illumination in order to avoid masking the trap capacitive
85 effects by the photocurrent. The voltage of the peak is shifted in
86 the cathodic direction when the scan rate increases, as indicated
87 by the gray arrow. The dependence of the cathodic peak
88 current with scan rate is linear, as shown in Figure 1d,
89 indicating that diffusion limitations do not exist for these
90 experiments. It should also be noticed that under dark
91 conditions at $V_0 = 1.66 \text{ V}$ versus RHE and at a scan rate of
92 500 mV/s (Figure 1a), the cathodic capacitive peak is hardly
93 visible, while under illumination, the peak is visible even at 50
94 mV/s .

95 The previous observations indicate that traps are created
96 chemically by oxidation of the hematite surface either by
97 imposing a higher positive bias or by illumination. It has been
98 suggested that these surface traps are $\text{Fe}=\text{O}$ intermediates and
99 the formation of these species by proton-coupled oxidation of
100 surface hydroxide species constitutes the first step of water
101 oxidation on hematite electrodes.^{16,25} In other materials, like
102 GaN for instance,²⁶ surface traps are mainly due to the
103 morphology of the material and are present in the dark and

under illumination. Consequently, in the latter situation, the 104
105 voltammetry plots display a comparable capacitive peak for
106 both pretreatments. Additionally, it should also be noted that
107 no anodic peak is present in any of the plots represented in
108 Figure 1a and c. However, it has been recently remarked²³ that
109 after deposition of an iridium-based catalyst to the hematite
110 surface, a quasi-symmetric peak can be observed at cathodic
111 V

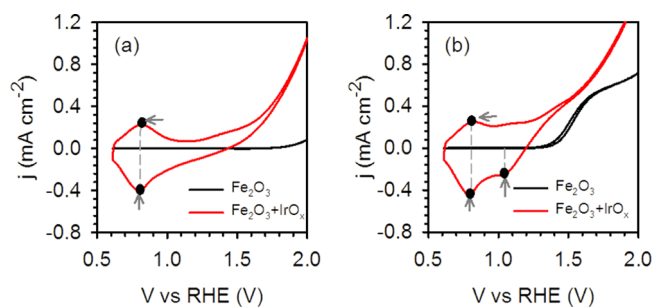


Figure 2. Cyclic voltammetry curves obtained in the dark (peak voltage: $V_1 = 0.8 \text{ V}$ versus RHE; capacitive peaks: $j_1^{\text{cat}} = -0.4 \text{ mA cm}^{-2}$, $j_1^{\text{an}} = 0.22 \text{ mA cm}^{-2}$) (a) and under illumination at 100 mW cm^{-2} (second peak voltage: $V_2 = 1.01 \text{ V}$ versus RHE; cathodic peak: $j_2^{\text{cat}} = -0.26 \text{ mA cm}^{-2}$) (b) for a reference Fe_2O_3 sample (black curve) and after electrodeposition of an IrO_x layer from a metallorganic $[\text{Cp}^*\text{Ir}(\text{H}_2\text{O})_3](\text{SO}_4)$ precursor (red curve). Surface concentration of Ir on Fe_2O_3 : 3.9 atom %. Scan rate: 10 mV s^{-1} .²³

both in the dark and under illumination conditions, indicates 112
113 that IrO_x acts in a similar fashion as intrinsic surface states, by
114 capture and release of carriers from those states, which
115 facilitates charge transfer to solution. This capacitive feature
116 of IrO_x can be obviously related to the standard CV behavior of
117 redox species. More specifically, it has been ascribed to an
118 Ir(III)/Ir(IV) redox process, which involves a two-electron,
119 three-proton process.^{27,28} However, it is interesting to discuss
120 how the redox catalyst is electronically coupled to the
121 semiconductor film. Similar observations have been reported
122 with cobalt–phosphate (Co–Pi) catalyst layers covering
123 hematite electrodes.¹⁵

In the following, we present a simple model that allows 124
125 prediction of the voltammetry plots in the presence of a
126 monoenergetic level of surface states with a pretreatment done
127 under illumination at a voltage above the onset voltage. The
128 model, which is based on a previous model developed by
129 Bisquert,²⁹ allows prediction of the voltammetry patterns
130 reported in the present study and, in general, in the
131 measurement of solar water splitting semiconductor films.

We consider a thin and homogeneous semiconductor film of 132
133 length d with a density of N_t monoenergetic traps per unit of
134 volume, as shown in Figure 3. We term n and f as the density of 134 B
135 electrons in the conduction band and the traps occupation
136 probability, respectively. n_0 and f_0 are the same respective
137 quantities taken at equilibrium. The detailed calculation of f_0 is
138 given in the Supporting Information (SI). Because the
139 distribution of carriers in the semiconductor layer is assumed
140 to be homogeneous, n only depends on time and is governed
141 by the applied voltage V

$$n(t) = n_0 \exp\left(-\frac{qV(t)}{k_B T}\right) \quad (1) \quad 142$$

where $k_B T$ is the thermal energy. 143

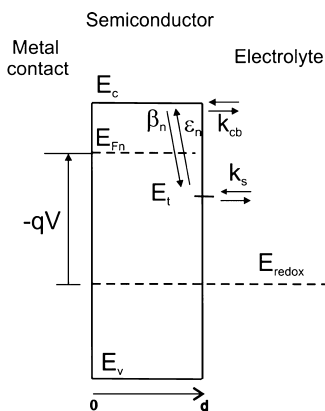


Figure 3. Scheme of the kinetics of the processes occurring at the interface of the semiconductor/solution. d is the thickness of the semiconductor layer. The processes are trapping of electrons from the conduction band (β_n) and detrapping (ϵ_n) and charge transfer of electrons from the traps (k_s) and from the conduction band (k_{cb}).

144 It is well-known that the presence of an electric field in the
145 space charge region improves charge separation in the active
146 layer, which can enhance the fuel production efficiency.¹² In the
147 model below, we address the question of trap occupation and
148 charge transfer from the surface states, depending on the
149 homogeneous electrode potential. The same model could be
150 formulated for a surface Schottky barrier with simple
151 modifications, but these considerations are beyond the scope
152 of this work. Henceforth, for the sake of simplicity, the
153 influence of the electric field at the interface of the electrolyte/
154 semiconductor is neglected.

155 Initially, before the voltammetry scan, a pretreatment is done
156 in order to fill the traps with holes at a fixed voltage V_0 more
157 positive than the current onset voltage. Therefore, when the
158 voltammetry sweep starts, that is, at $t = 0$, we consider that
159 $f(t=0) = 0$. For a more complete treatment, $f(t=0)$ should be
160 calculated by taking into account both electron and hole
161 recombination and charge transfer from traps. However, for
162 simplicity, the dynamics of holes are not included in Figure 3.
163 For the interested reader, such calculations can be found in ref
164 20 for the technique of IS.

165 During the cyclic voltammetry scan, that is, at time $t > 0$, the
166 semiconductor is in the dark. Two types of processes are
167 considered in this case, (i) charge transfer from the conduction
168 band (kinetic constant k_{cb}) and from the traps (k_s) and (ii)
169 electron trapping (β_n)/detrapping (ϵ_n). We aim to calculate the
170 current density j_n , and we use the usual boundary conditions, eq
171 1 at the left metal/semiconductor contact, and at the right, the
172 semiconductor/electrolyte contact is considered to be a
173 blocking layer (i.e., $j_n(d,t) = 0$). The voltage that appears in
174 eq 1 varies with time as

$$175 \begin{cases} V(t \leq \lambda) = V_0 - st \\ V(t \geq \lambda) = V_0 - 2s\lambda + st \end{cases} \quad (2)$$

176 where s is the scan rate and λ the period of the voltage sweep.
177 Integration of the continuity equation for electrons in the
178 conduction band and the master equation for electrons in the
179 traps along the homogeneous layer of length d leads to

$$180 \frac{\partial n}{\partial t} = -\frac{1}{qd}j_n(0) - \beta_n(1-f)nN_t + \epsilon_n f N_t - k_{cb}(n - n_0) \quad (3)$$

$$\frac{\partial f}{\partial t} + \epsilon_n + k_s(1 - f_0) = (\beta_n n + \epsilon_n + k_s)(1 - f) \quad (4) \quad 181$$

We shall introduce some useful quantities, namely, the
182 equilibrium chemical capacitances^{30,31} associated with each
183 charge storage mode. We define the well-known chemical
184 capacitance for electrons in the conduction band
185

$$C_{\mu}^{cb} = qd \left| \frac{\partial n}{\partial V} \right| = \frac{q^2 d}{kT} n \quad (5) \quad 186$$

and the equilibrium chemical capacitance of the traps^{32–34}
187

$$C_{\mu eq}^{ss} = qd \left| \frac{\partial f}{\partial V} \right| N_t \quad (6) \quad 188$$

Note that the latter capacitance relies on the knowledge of f ,
189 which relies on the resolution of eq 4. Equations 2–4 provide
190 the general form of the voltammetric current
191

$$\begin{cases} j_n(t \leq \lambda) = j_{res} - j_{cap} \\ j_n(t \geq \lambda) = j_{res} + j_{cap} \end{cases} \quad (7) \quad 192$$

where j_{res} is the resistive current density (i.e., faradaic current)
193

$$j_{res} = -qd \left[k_{cb} + (1 - B)\epsilon_n \frac{N_t}{n_0} f_0 \right] \times (n - n_0) \quad (8) \quad 194$$

with
195

$$B = 1 - \frac{k_s}{\beta_n n + \epsilon_n + k_s} \quad (9) \quad 196$$

j_{cap} is the capacitive current density given by
197

$$j_{cap} = [C_{\mu}^{cb} + BC_{\mu eq}^{ss}] \times s \quad (10) \quad 198$$

The first term on the right-hand side of eq 8 corresponds to the
199 charge transfer from the conduction band, while the second
200 term has already been associated through IS to the trapping/
201 detrapping process and charge transfer from the traps.²⁹
202

The general solution of the above set of equations can be
203 obtained numerically, but it is useful to distinguish between
204 different physical cases. In the model of Figure 3, we will
205 consider that charge transfer from the traps is slow enough
206 compared to the velocity of trap charging so that a capacitance
207 peak can be observed. This implies that $k_s \ll qs/k_B T$. Note that
208 in the case where charge transfer from the traps is zero ($k_s = 0$),
209 the following treatment can also be applied for the bulk of the
210 semiconductor if it is homogeneous enough so that eqs 3 and 4
211 remain valid. However, this latter case is not desired for fuel
212 production because it would imply high onset voltages. Besides,
213 as indicated by the experimental CV patterns of Figures 1 and
214 2, it is important to distinguish two types of behaviors; either
215 trapping/detrapping is fast enough in comparison with the trap
216 charging velocity, that is, $\epsilon_n \gg qs/k_B T$ or inversely.
217

In the case where trapping/detrapping is very fast, traps are
218 in equilibrium with the semiconductor conduction band, while
219 in the second case, electrons accumulate in the traps and are
220 therefore subject to much higher recombination. In the first
221 case, the onset voltage should therefore be lower than that in
222 the second one. Let us now examine both cases in terms of the
223 voltammetry pattern and relate them to the experimental cases
224 depicted by Figures 1 and 2.
225

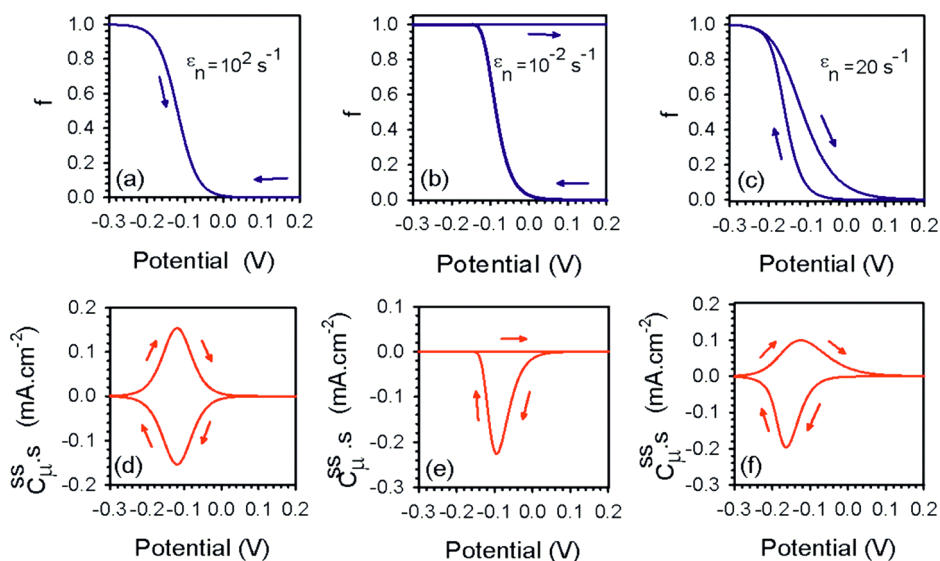


Figure 4. Trap occupation probability for a system limited by charge transfer and (a) when detrapping is fast with respect to the charging velocity (i.e., traps are in equilibrium with the conduction band), (b) when detrapping is slow (i.e., high recombination), and (c) for an intermediary case. (d–f) Trap capacitive current derived from the respective occupation probability of (a–c). Simulation parameters: $kT = 26$ meV, $d = 1$ nm, $N_t = 10^{21}$ cm^{-3} , $\beta_n n_0 = 1$ s^{-1} , $k_s = 10^{-4}$ s^{-1} , $s = 1$ $\text{V}\cdot\text{s}^{-1}$.

In Figure 4, we give examples of representation of the trap occupation probability f for a system limited by charge transfer. We illustrate three cases, when detrapping is fast, depicted in Figure 4a, when detrapping is slow, shown in Figure 4b, and an intermediary case represented in Figure 4c. The corresponding capacitive currents (sC_{μ}^{ss}) from the traps are given in Figure 4d–f. In Figure 5, we give the total voltammetric current obtained from the numerical resolution of eqs 3 and 4 in different cases discussed below.

We now discuss the influence of the trap kinetics on the voltammetry patterns for semiconductors used for water splitting applications. We focus on the possible shapes of the CV patterns obtained in the framework of our model. We then compare them to both experimental examples of Figures 1 and 2, which are representative of the main voltammetry plots that can be found in the literature for this type of system.

When the voltammetry scan is carried out in the cathodic direction, the electron Fermi level is shifted upward, and traps (initially filled with holes because of the pretreatment) are filled with electrons while the conduction band is filled at more cathodic voltage. The voltammetry pattern therefore displays a first cathodic capacitive peak induced by the filling of the traps by electrons followed either by the faradic current from the conduction band (Figure 5b and d) or by the capacitive current (Figures 5a and c). In the anodic direction, because charge transfer from the traps is slow with respect to the trap charging velocity, traps are emptied relatively according to the detrapping rate.

In the case where detrapping is very slow (Figure 5a and b) with respect to the trap charging velocity, charges accumulate in the traps in the cathodic direction. Note that in this case, the voltage of the cathodic peak depends on the scan rate and is shifted toward the cathodic direction as the scan rate increases. The mathematical demonstration of this result is given in the SI. In the anodic direction, because detrapping is very slow, the charges accumulated in the traps are extracted much slower than they were injected in the cathodic direction. For this reason, the occupation probability is almost constant and maximum in the anodic direction (Figure 4b). As a

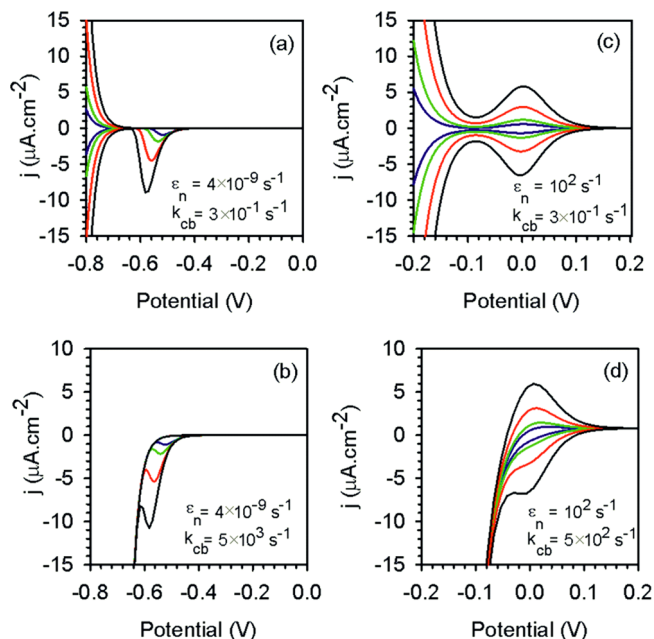


Figure 5. Voltammetric plots obtained by solving numerically eqs 3 and 4 under the condition that charge transfer is a limiting kinetic factor. Four different cases are computed where detrapping ($\epsilon_n = \beta_n n_0$) and charge transfer from the conduction band (k_{cb}) are analyzed. The general parameters of this simulation are $kT = 26$ meV, $d = 1$ nm, $N_t = 8 \times 10^{19}$ cm^{-3} , $k_s = 10^{-2}$ s^{-1} . For each figure, the blue plot corresponds to the scan rate 50 $\text{mV}\cdot\text{s}^{-1}$, the green plot to 100 $\text{mV}\cdot\text{s}^{-1}$, the red plot to 250 $\text{mV}\cdot\text{s}^{-1}$, and the black one to 500 $\text{mV}\cdot\text{s}^{-1}$.

consequence, no anodic peak can be observed. Experimentally, this latter case is depicted by Figure 1 for bare hematite. In this case, traps are formed by oxidation of the hematite surface. The shape of the capacitive peak that appears after illumination of the sample indicates that not only is the charge transfer from the traps slow, but also, the detrapping process is sluggish. Thereby, traps actuate as recombination centers and limit the oxygen evolution. The same behavior has been reported in the

273 case of GaN.²⁶ Nonetheless, in this case, surface states are
274 intrinsic and display a capacitive peak in both dark and
275 illumination conditions, though the peak intensity is higher
276 under illumination compared to that under dark conditions.
277 This is due to the fact that in the dark, those surface states are
278 initially partially filled with electrons, while under illumination,
279 traps are emptied by hole trapping, which allows for higher
280 charge accumulation during the voltammetry sweep.

281 In the case where both trapping and detrapping are fast
282 compared to the trap charging velocity (Figure 5c and d),
283 charge accumulation is reversible, and the occupation
284 probability is equal in both the anodic and cathodic directions
285 (Figure 4a). Hence, the trap capacitance is the same in both
286 directions, and the trap capacitive current is symmetric and
287 proportional to the scan rate (see the SI for more information
288 on the capacitance peak voltage). This situation corresponds to
289 the experimental case depicted by Figure 2. When the hematite
290 surface is treated with an iridium-based catalyst, two quasi-
291 symmetric peaks, cathodically shifted with respect to the bare
292 hematite peak, appear under both dark and illumination
293 conditions. This indicates that IrO_x highly reversible oxidation
294 states act similarly to intrinsic surface states and that detrapping
295 is much easier in this case. Consequently, the IrO_x catalyst
296 enhances the detrapping process and decreases recombination.
297 For this reason, higher currents and lower onset voltages can be
298 achieved.³⁵ It has also been shown by IS that IrO_x enhances
299 charge transfer.²³ Additionally, it should be remarked that a
300 second cathodic peak appears under illumination. We believe
301 that this peak corresponds to the surface states created by
302 oxidation of the hematite surface, as already observed for bare
303 hematite. It should also be remarked that in other recent
304 studies, the capacitive response of surface states has been found
305 to be reduced in the presence of Ga₂O₃ and Al₂O₃
306 overlayers.^{36,37} It has been suggested that 13-group oxide
307 overlayers passivate surface states by releasing lattice strain of
308 the hematite layer. On the other hand, the deposition of cobalt-
309 based catalyst layers also leads to a decrease of surface state
310 capacitance by accelerating the charge-transfer rate from surface
311 states.³⁸ It should be mentioned that these previous studies
312 were carried out under illumination, and consequently, the
313 capacitive response of the electrodes was partially masked by
314 the photocurrent, in contrast with our present study in dark
315 conditions.

316 In conclusion, we have shown that when charge transfer is
317 very slow, at least one capacitive peak can be observed in the
318 voltammograms corresponding to the system at stake. The
319 presence of one capacitive peak only in the cathodic direction
320 (i.e., without the corresponding symmetric anodic peak) is a
321 feature of a system exhibiting high recombination. In this case,
322 the peak voltage is shifted in the cathodic direction as the scan
323 rate increases. On the contrary, two symmetric peaks
324 characterize a system with trap states in equilibrium with the
325 conduction band and display lower recombination compared to
326 the previous case. In this case, both peaks increase propor-
327 tionally to the scan rate, and the peak voltage is constant with
328 scan rate. A system that is characterized by a good charge
329 transfer from traps does not display any capacitive peak.

330 ■ ASSOCIATED CONTENT

331 ● Supporting Information

332 The detailed calculation of the trap occupation probability at
333 equilibrium and the capacitance peak voltage observed in the
334 CV patterns in both cases of slow and fast trapping/detrapping

with respect to the trap charging velocity. This material is 335
available free of charge via the Internet at <http://pubs.acs.org>. 336

337 ■ AUTHOR INFORMATION

338 Corresponding Author

339 *E-mail: bisquert@uji.es.

340 Notes

341 The authors declare no competing financial interest.

342 ■ ACKNOWLEDGMENTS

343 The research leading to these results is supported by 343
Universitat Jaume I Project P1-1B2011-50. 344

345 ■ REFERENCES

- 346 (1) Bolts, J.; Wrighton, M. Correlation of Photocurrent–Voltage 346
Curves with Flat-Band Potential Stable Photoelectrodes for the 347
Photoelectrolysis of Water. *J. Phys. Chem.* **1976**, *80*, 2641–2645. 348
- 349 (2) Nozik, A. J. Photoelectrochemistry: Applications to Solar Energy 349
Conversion. *Annu. Rev. Phys. Chem.* **1978**, *29*, 189. 350
- 351 (3) Butler, M. A.; Ginley, D. S. Principles of Photoelectrochemical, 351
Solar Energy Conversion. *J. Mater. Sci.* **1980**, *15*, 1–19. 352
- 353 (4) Walter, M. G.; Warren, E. L.; McKone, J. R.; Boettcher, S. W.; 353
Mi, Q. X.; Santori, E. A.; Lewis, N. S. Solar Water Splitting Cells. 354
Chem. Rev. **2010**, *110*, 6446–6473. 355
- 356 (5) Kennedy, J. H. Photooxidation of Water at α -Fe₂O₃ Electrodes. *J.* 356
Electrochem. Soc. **1978**, *125*, 709. 357
- 358 (6) Murphy, A.; Barnes, P.; Randeniya, L.; Plumb, I.; Grey, I.; Horne, 358
M.; Glasscock, J. Efficiency of Solar Water Splitting Using Semi- 359
conductor Electrodes. *Int. J. Hydrogen Energy* **2006**, *31*, 1999–2017. 360
- 361 (7) Dare-Edwards, M. P.; Goodenough, J. B.; Hamnett, A.; 361
Trevellick, P. R. Electrochemistry and Photoelectrochemistry of 362
Iron(III) Oxide. *J. Chem. Soc., Faraday Trans. 1* **1983**, *79*, 2027–2041. 363
- 364 (8) Katz, M. J.; Riha, S. C.; Jeong, N. C.; Martinson, A. B. F.; Farha, 364
O. K.; Hupp, J. T. Toward Solar Fuels: Water Splitting with Sunlight 365
and Rust? *Coord. Chem. Rev.* **2012**, *256*, 2521–2529. 366
- 367 (9) Peter, L. M. Energetics and Kinetics of Light-Driven Oxygen 367
Evolution at Semiconductor Electrodes: The Example of Hematite. *J.* 368
Solid State Electrochem. **2012**, *17*, 315–326. 369
- 370 (10) Barroso, M.; Cowan, A. J.; Pendlebury, S. R.; Gratzel, M.; Klug, 370
D. R.; Durrant, J. R. The Role of Cobalt Phosphate in Enhancing the 371
Photocatalytic Activity of α -Fe₂O₃ toward Water Oxidation. *J. Am.* 372
Chem. Soc. **2011**, *133*, 14868–14871. 373
- 374 (11) Zhong, D. K.; Choi, S.; Gamelin, D. R. Near-Complete 374
Suppression of Surface Recombination in Solar Photoelectrolysis by 375
“Co–Pi” Catalyst-Modified W:BiVO₄. *J. Am. Chem. Soc.* **2011**, *133*, 376
18370–18377. 377
- 378 (12) Barroso, M.; Mesa, C. A.; Pendlebury, S. R.; Cowan, A. J.; 378
Hisatomi, T.; Sivula, K.; Gratzel, M.; Klug, D. R.; Durrant, J. R. 379
Dynamics of Photogenerated Holes in Surface Modified α -Fe₂O₃ 380
Photoanodes for Solar Water Splitting. *Proc. Natl. Acad. Sci. U.S.A.* 381
2012, *109*, 15640–15645. 382
- 383 (13) Wijayantha, K. G. U.; Saremi-Yarahmadia, S.; Peter, L. M. 383
Kinetics of Oxygen Evolution at α -Fe₂O₃ Photoanodes: A Study by 384
Photoelectrochemical Impedance Spectroscopy. *Phys. Chem. Chem.* 385
Phys. **2010**, *13*, 5264–5270. 386
- 387 (14) Peter, L. M.; Wijyantha, K. G. U.; Tahir, A. A. Kinetics of 387
Light-Driven Oxygen Evolution at α -Fe₂O₃ Electrodes. *Faraday* 388
Discuss. **2012**, *155*, 309–322. 389
- 390 (15) Klahr, B.; Gimenez, S.; Fabregat-Santiago, F.; Bisquert, J.; 390
Hamann, T. W. Photoelectrochemical and Impedance Spectroscopic 391
Investigation of Water Oxidation with Co–Pi-Coated Hematite 392
Electrodes. *J. Am. Chem. Soc.* **2012**, *134*, 16693–16700. 393
- 394 (16) Klahr, B.; Gimenez, S.; Fabregat-Santiago, F.; Bisquert, J.; 394
Hamann, T. W. Electrochemical and Photoelectrochemical Inves- 395
tigation of Water Oxidation with Hematite Electrodes. *Energy. Environ.* 396
Sci. **2012**, *5*, 7626. 397

- 398 (17) Braun, A.; Sivula, K.; Bora, D. K.; Zhu, J.; Zhang, L.; Grätzel, M.;
399 Guo, J.; Constable, E. C. Direct Observation of Two Electron Holes in
400 a Hematite Photo-Anode During Photo-Electrochemical Water
401 Splitting. *J. Phys. Chem. C* **2012**, *116*, 16870–16875.
- 402 (18) Vanmaekelbergh, D.; Cardon, F. Calculation of the Electrical
403 Impedance Associated with the Surface Recombination of Free
404 Carriers at an Illuminated Semiconductor/Electrolyte Interface. *J.*
405 *Phys. D: Appl. Phys.* **1986**, *19*, 643.
- 406 (19) Ponomarev, E. A.; Peter, L. M. A Comparison of Intensity
407 Modulated Photocurrent Spectroscopy and Photoelectrochemical
408 Impedance Spectroscopy in a Study of Photoelectrochemical Hydro-
409 gen Evolution at p-InP. *J. Electrochem. Chem.* **1995**, *397*, 45–52.
- 410 (20) Bertoluzzi, L.; Bisquert, J. Equivalent Circuit of Electrons and
411 Holes in Thin Semiconductor Films for Photoelectrochemical Water
412 Splitting Applications. *J. Phys. Chem. Lett.* **2012**, *3*, 2517–2522.
- 413 (21) Fabregat-Santiago, F.; Mora-Seró, I.; Garcia-Belmonte, G.;
414 Bisquert, J. Cyclic Voltammetry Studies of Nanoporous Semi-
415 conductor Electrodes. Models and Application to Nanocrystalline
416 TiO₂ in Aqueous Electrolyte. *J. Phys. Chem. B* **2003**, *107*, 758–769.
- 417 (22) Kay, A.; Cesar, I.; Grätzel, M. New Benchmark for Water
418 Photooxidation by Nanostructured α -Fe₂O₃ Films. *J. Am. Chem. Soc.*
419 **2006**, *128*, 15714–15721.
- 420 (23) Badia-Bou, L.; Mas Marzá, E.; Rodenas, P.; Barea, E. M.;
421 Fabregat-Santiago, F.; Gimenez, S.; Peris, E. V.; Bisquert, J. Water
422 Oxidation at Hematite Photoelectrodes with an Iridium Based
423 Catalyst. *J. Phys. Chem. C* **2013**, *117*, 3826–3833.
- 424 (24) Jaegermann, W. The Semiconductor/Electrolyte Interface: A
425 Surface Science Approach. In *Modern Aspects of Electrochemistry*;
426 White, R. E., Ed.; Plenum Press: New York, 1996; No. 30.
- 427 (25) Hellman, A.; Pala, R. G. S. A First-Principles Study of Photo-
428 Induced Water-Splitting on Fe₂O₃. *J. Phys. Chem. C* **2011**, *115*,
429 12901–12907.
- 430 (26) Schäfer, S.; Koch, A. H. R.; Cavallini, A.; Stutzmann, M.; Sharp,
431 I. D. Charge Transfer across the n-Type GaN–Electrolyte Interface. *J.*
432 *Phys. Chem. C* **2012**, *116*, 22281–22286.
- 433 (27) Blakemore, J. D.; Schley, N. D.; Olack, G. W.; Incarvito, C. D.;
434 Brudvig, G. W.; Crabtree, R. H. Anodic Deposition of a Robust
435 Iridium-Based Water-Oxidation Catalyst from Organometallic Pre-
436 cursors. *Chem. Sci.* **2011**, *2*, 94–98.
- 437 (28) Burke, L. D.; Whelan, D. P. A New Interpretation of the Charge
438 Storage and Electrical-Conductivity Behavior of Hydrous Iridium
439 Oxide. *J. Electroanal. Chem.* **1981**, *124*, 333–337.
- 440 (29) Bisquert, J. Theory of the Impedance of Charge Transfer via
441 Surface States in Dye-Sensitized Solar Cells. *J. Electrochem. Chem.*
442 **2010**, *646*, 43–51.
- 443 (30) Bisquert, J. Chemical Capacitance of Nanostructured Semi-
444 conductors: Its Origin and Significance for Heterogeneous Solar Cells.
445 *Phys. Chem. Chem. Phys.* **2003**, *5*, 5360–5364.
- 446 (31) Bisquert, J. Beyond the Quasi-Static Approximation: Impedance
447 and Capacitance of an Exponential Distribution of Traps. *Phys. Rev. B*
448 **2008**, *77*, 235203.
- 449 (32) Frese, K. W.; Morrison, S. R. Electrochemical Measurements of
450 Interface States at the GaAs/Oxide Interface. *J. Electrochem. Soc.* **1979**,
451 *126*, 1235–1241.
- 452 (33) Dare-Edwards, M. P.; Hamnett, A.; Trevellick, P. R. Alternating-
453 Current Techniques in Semiconductor Electrochemistry. *J. Chem. Soc.*,
454 *Faraday Trans. 1* **1983**, *79*, 2111–2124.
- 455 (34) Allongue, P.; Cachet, H. I–V Curve and Surface State
456 Capacitance at Illuminated Semiconductor/Liquid Contacts. *J. Electro-*
457 *chem. Chem.* **1984**, *176*, 369–375.
- 458 (35) Tilley, S. D.; Cornuz, M.; Sivula, K.; Grätzel, M. Light-Induced
459 Water Splitting with Hematite: Improved Nanostructure and Iridium
460 Oxide Catalysis. *Angew. Chem., Int. Ed.* **2010**, *49*, 6405–6408.
- 461 (36) Le Formal, F.; Sivula, K.; Grätzel, M. The Transient
462 Photocurrent and Photovoltage Behavior of a Hematite Photoanode
463 under Working Conditions and the Influence of Surface Treatments. *J.*
464 *Phys. Chem. C* **2012**, *116*, 26707–26720.
- 465 (37) Hisatomi, T.; Le Formal, F.; Cornuz, M.; Brillet, J.; Tetreault,
466 N.; Sivula, K.; Grätzel, M. Cathodic Shift in Onset Potential of Solar
Oxygen Evolution on Hematite by 13-Group Oxide Overlayers. *Energy* **2011**, *4*, 2512–2515.
- (38) Riha, S. C.; Klahr, B. M.; Tyo, E. C.; Seifert, S.; Vajda, S.; Pellin,
M. J.; Hamann, T. W.; Martinson, A. B. F. Atomic Layer Deposition of
a Submonolayer Catalyst for the Enhanced Photoelectrochemical
Performance of Water Oxidation with Hematite. *ACS Nano* **2013**, *7*,
2396–2405.